
Figures and figure supplements

FAK loss reduces BRAF^{V600E}-induced ERK phosphorylation to promote intestinal stemness and cecal tumor formation

Chenxi Gao *et al.*

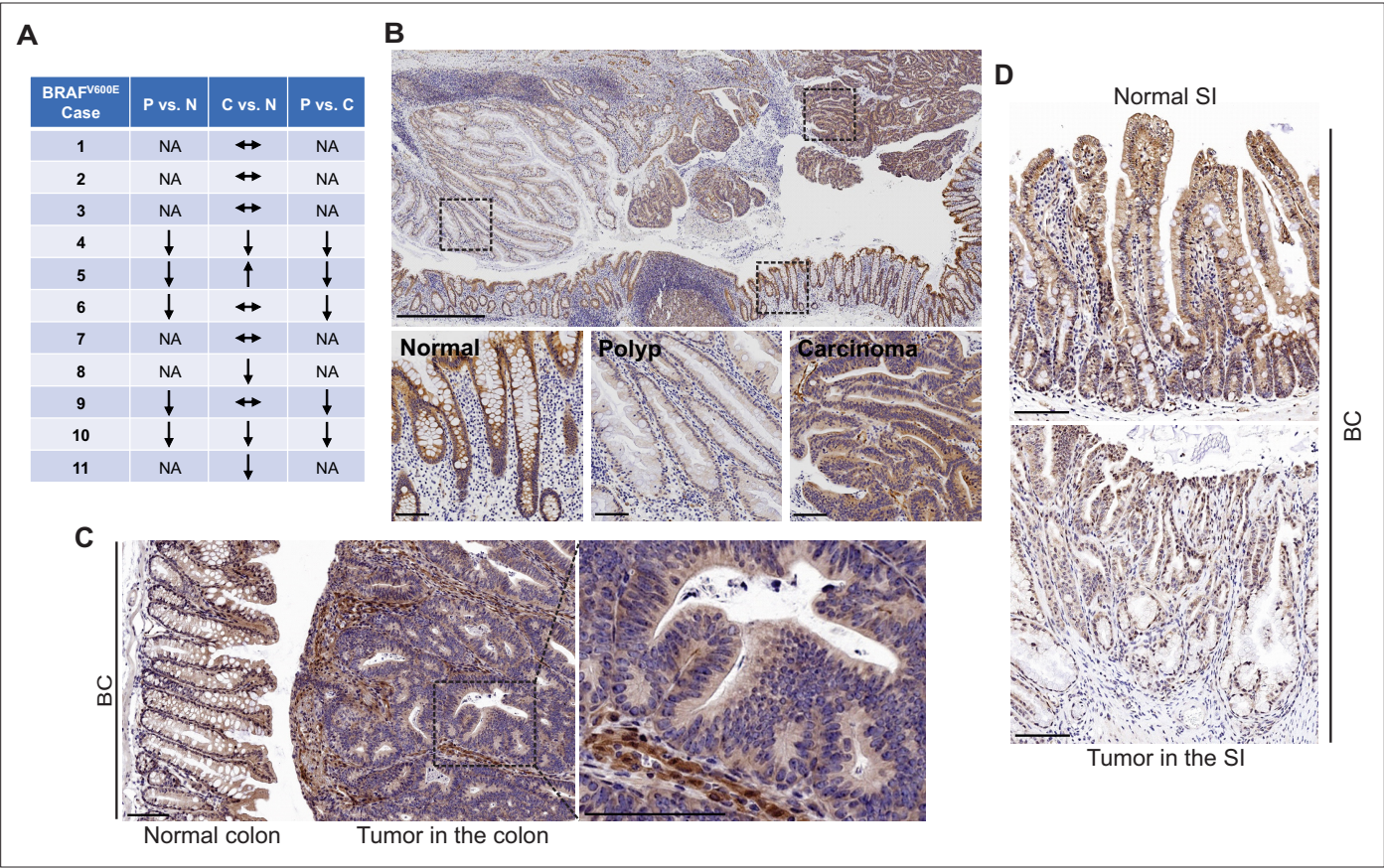


Figure 1. FAK downregulation in serrated tumors. **(A)** Summary of FAK IHC staining in 11 human $BRAF^{V600E}$ -mutant CRC samples. N represents normal colon; P represents polyp; C represents carcinoma; NA, not applicable; ↔ represents no change; ↑ represents an increase. ↓ represents a decrease. **(B)** Representative IHC staining of $BRAF^{V600E}$ -mutant patient SSA/P, serrated colorectal adenoma, and adjacent normal tissues. **(C)** IHC staining of Fak in small intestine tumors in a 12-month-old BC mouse. **(D)** Representative IHC staining of Fak in colon tumor in 12-month-old BC mice. Scale bars in **(B)** 1 mm (upper panel) and 100 μm (lower panel). Scale bars in **(C)** and **(D)** 100 μm.

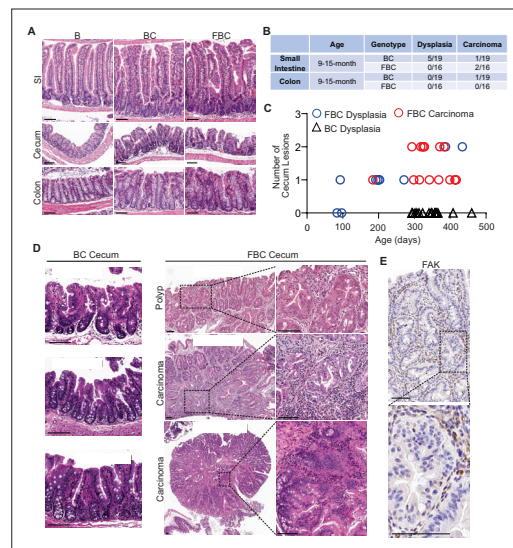


Figure 2. *Fak* loss enhances *BRAF*^{V600E}-driven cecal tumorigenesis in mice. (A) Representative hematoxylin and eosin (H&E) staining of the small intestine, cecum, and colon from indicated 6-week-old mice. (B) Summary of tumor incidence at small intestine and colon in indicated mice at the indicated age. (C) Summary of tumor incidence and tumor stage at indicated mice at the indicated age. (D) H&E staining of the cecum in BC mice and cecal serrated adenoma/polyp and carcinoma in FBC mice at the indicated age. (E) Representative IHC staining of *Fak* in cecal tumors in FBC mice. Scale bars: 100 μ m.

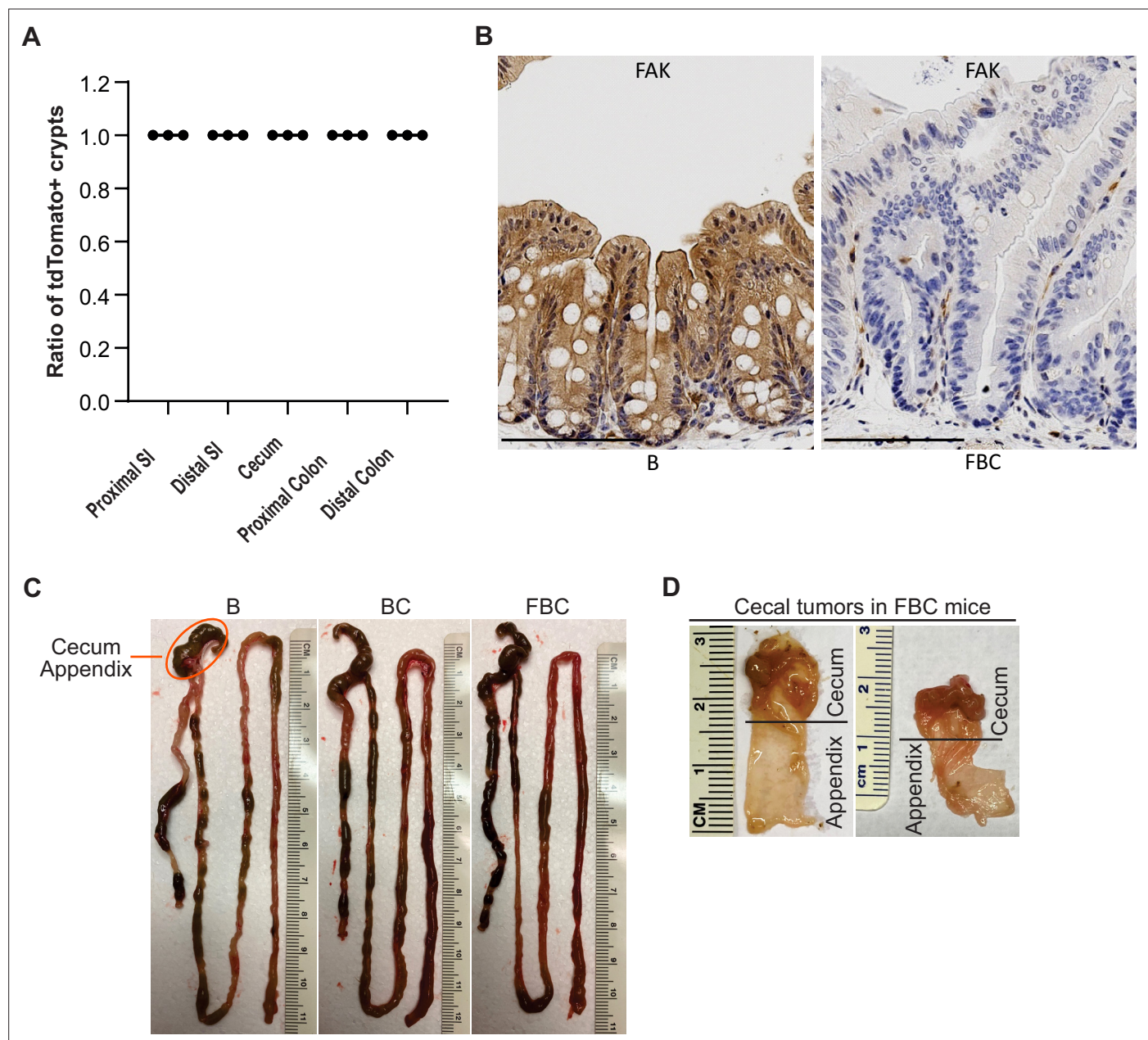


Figure 2—figure supplement 1. Fak deletion promotes *BRAF*^{V600E}-induced cecal tumorigenesis. **(A)** Cre-mediated recombination efficiency in *Villin-Cre; Rosa26*^{LSL-tdTomato/+} mice were scored for 30 crypts at each indicated bowel subsites (n=3). **(B)** Representative IHC staining of Fak in the cecum from B and FBC mice. **(C)** Representative examples of intestinal tracts in indicated 6-week-old mice. **(D)** Representative cecal tumors in 11–13-month-old FBC mice.

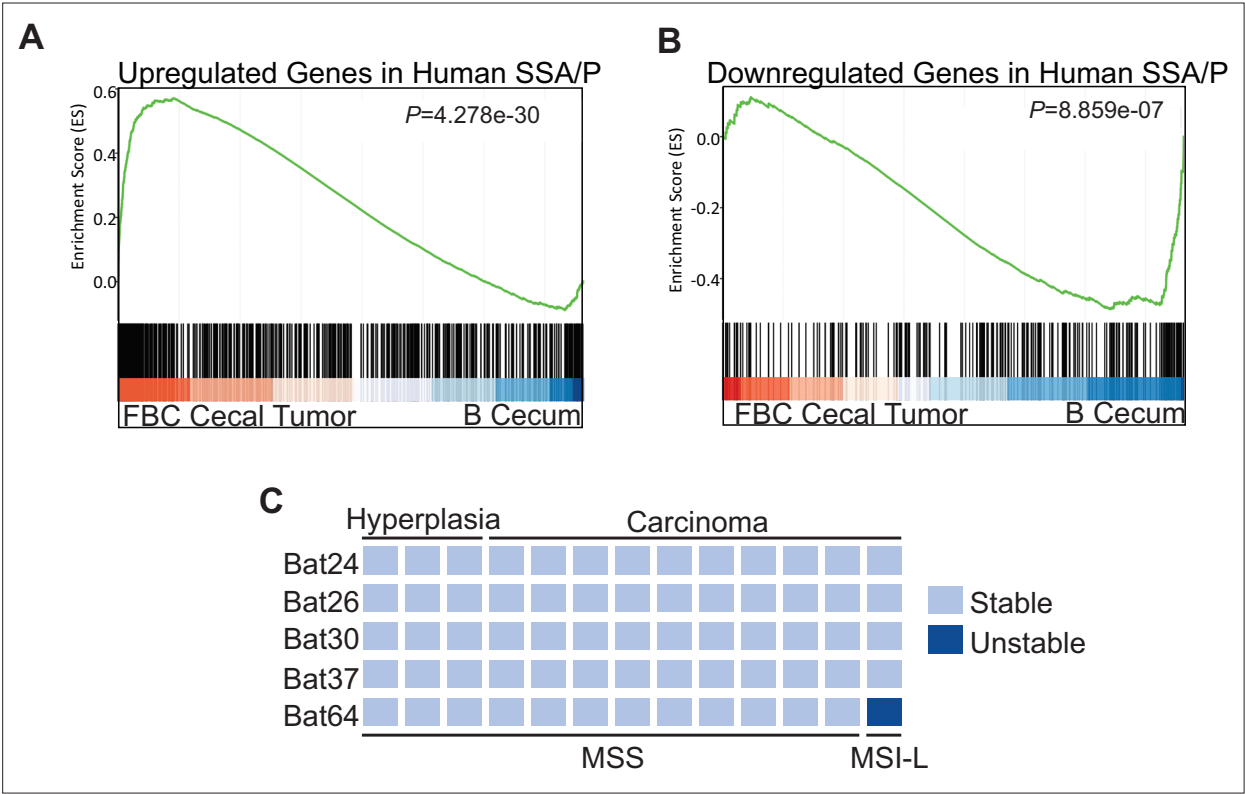


Figure 3. Molecular characterization of cecal tumors in FBC mice. **(A)** GSEA plot showing enrichment of human SSA/Ps signature genes (upregulated genes in SSA/Ps) in FBC cecal tumors vs normal cecal mucosa of B mice. **(B)** GSEA plot showing that downregulated genes in human SSA/Ps were also reduced in FBC cecal tumors. **(C)** Microsatellite instability status of FBC mice cecal mucosa and cecal carcinomas. Each column represents one sample.

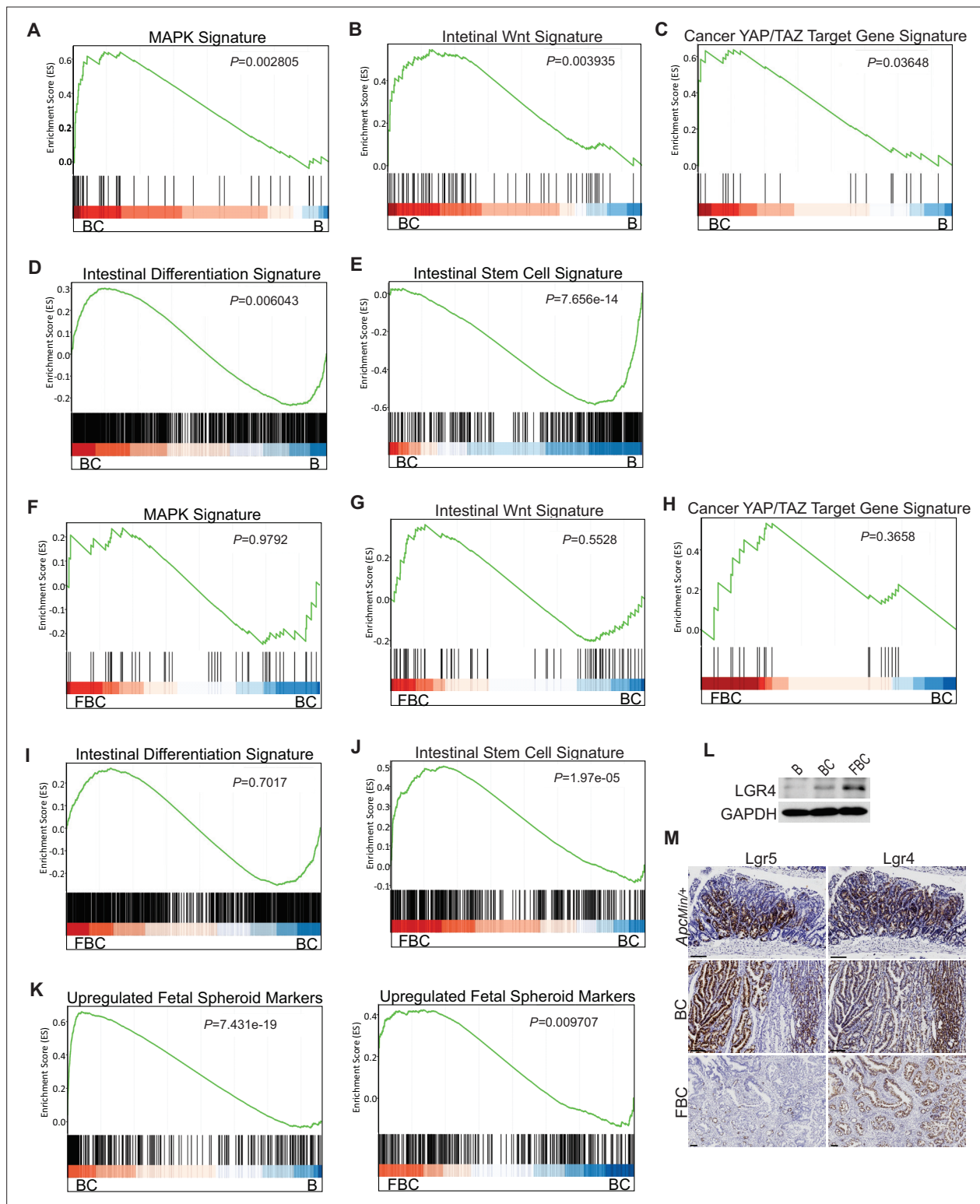


Figure 4. *BRAF*^{V600E} mutation and *Ptk2* loss-mediated changes in signaling pathways. GSEA analysis showing upregulation of MAPK signature (A), intestinal WNT signaling (B), YAP/TAZ target gene signature (C) and intestinal differentiation signature (D), and downregulation of intestinal stem cell signature (E) in the cecum of BC mice vs B mice (n=4 per group). GSEA plots revealed no significant change in MAPK signature (F), intestinal WNT signaling (G), YAP/TAZ target gene signature (H), and intestinal differentiation signature (I) in the cecum of FBC mice vs BC mice, but enrichment of stem cell signature in FBC mice (J) (n=4 per group). (K) GSEA analysis showing upregulation of upregulated fetal spheroid markers in the cecum of BC mice vs B mice, and further enrichment in the cecum of FBC mice vs BC mice (n=4 per group). (L) Immunoblotting analysis of LGR4 in the cecum from

Figure 4 continued on next page

Figure 4 continued

indicated 6-week-old mice. **(M)** Representative in situ hybridization (ISH) staining of tumor sections from *Apc*^{Min/+}, BC, and FBC mice using *Lgr4* and *Lgr5* probes. Scale bars: 100 μ m.

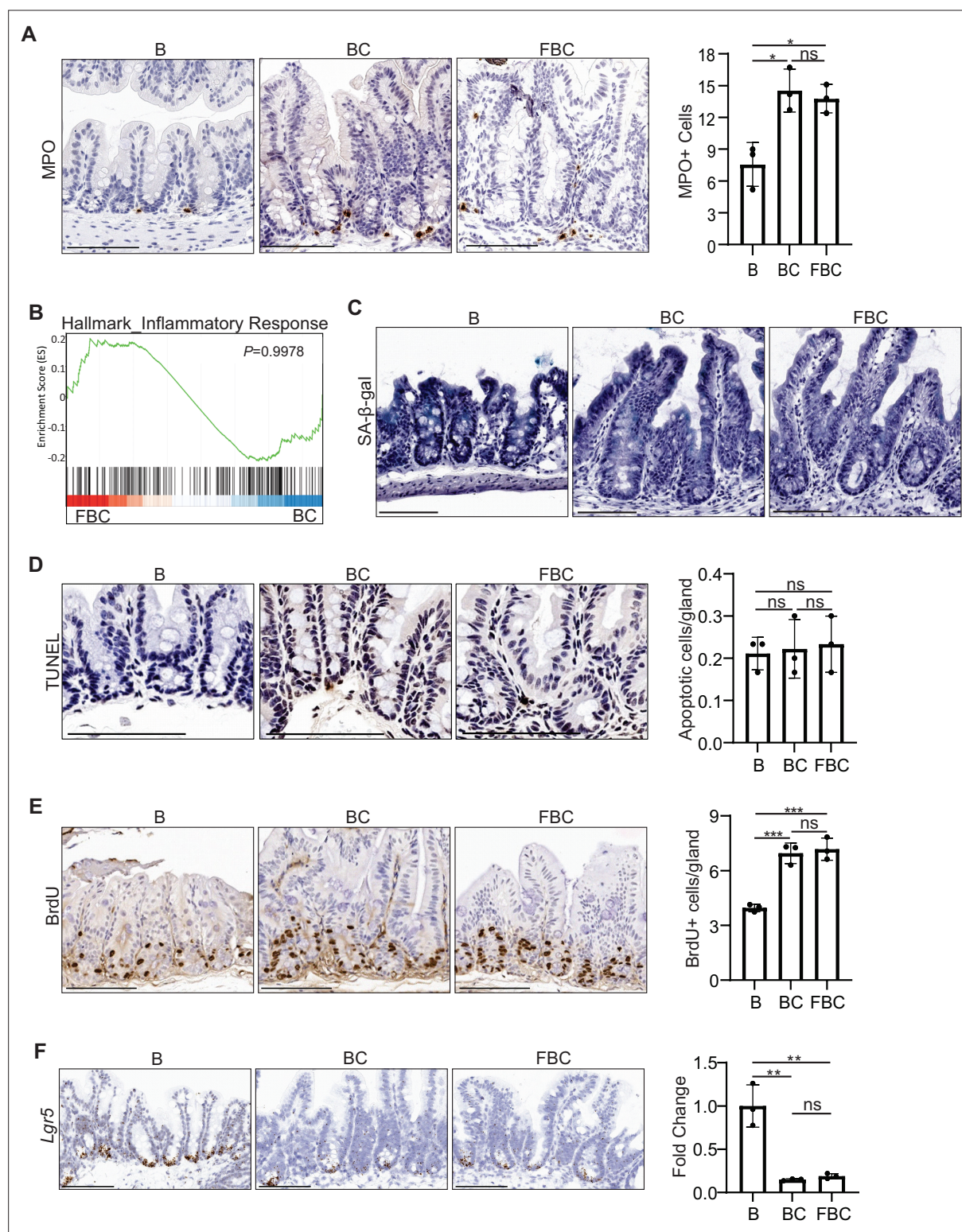


Figure 4—figure supplement 1. *Fak* loss has no impact on inflammation, senescence, apoptosis, proliferation, and *Lgr5* expression in the cecum in FBC mice. (A) Left panel: representative IHC staining of MPO in indicated mice. Right panel: quantification of MPO⁺ cells per 500 μ m-length of cecum on the tissue sections from indicated mice ($n=3$ per group). (B) GSEA plots reveal no change of inflammatory response gene signature in the cecum of FBC mice vs BC mice. (C) SA- β -galactosidase staining in indicated mice. (D) Left panel: representative images of TUNEL staining in indicated mice. Right panel: quantification of apoptotic cells per gland in cecum from indicated mice ($n=3$ per group). (E) Left panel: representative IHC staining of BrdU in indicated mice. Right panel: quantification of BrdU⁺ cells per gland in cecum from indicated mice ($n=3$ per group). (F) Left panel: representative RNA in

Figure 4—figure supplement 1 continued on next page

Figure 4—figure supplement 1 continued

situ hybridization (ISH) staining of *Lgr5* in indicated mice. Right panel: qRT-PCR of *Lgr5* in cecum from indicated mice (n=3 per group). All samples were collected from 6-week-old mice. Data presented as mean \pm SD (ns, not significant; *p<0.05; **p<0.01; ***p<0.001, Student's t-test, two-tailed). Scale bars: 100 μ m.

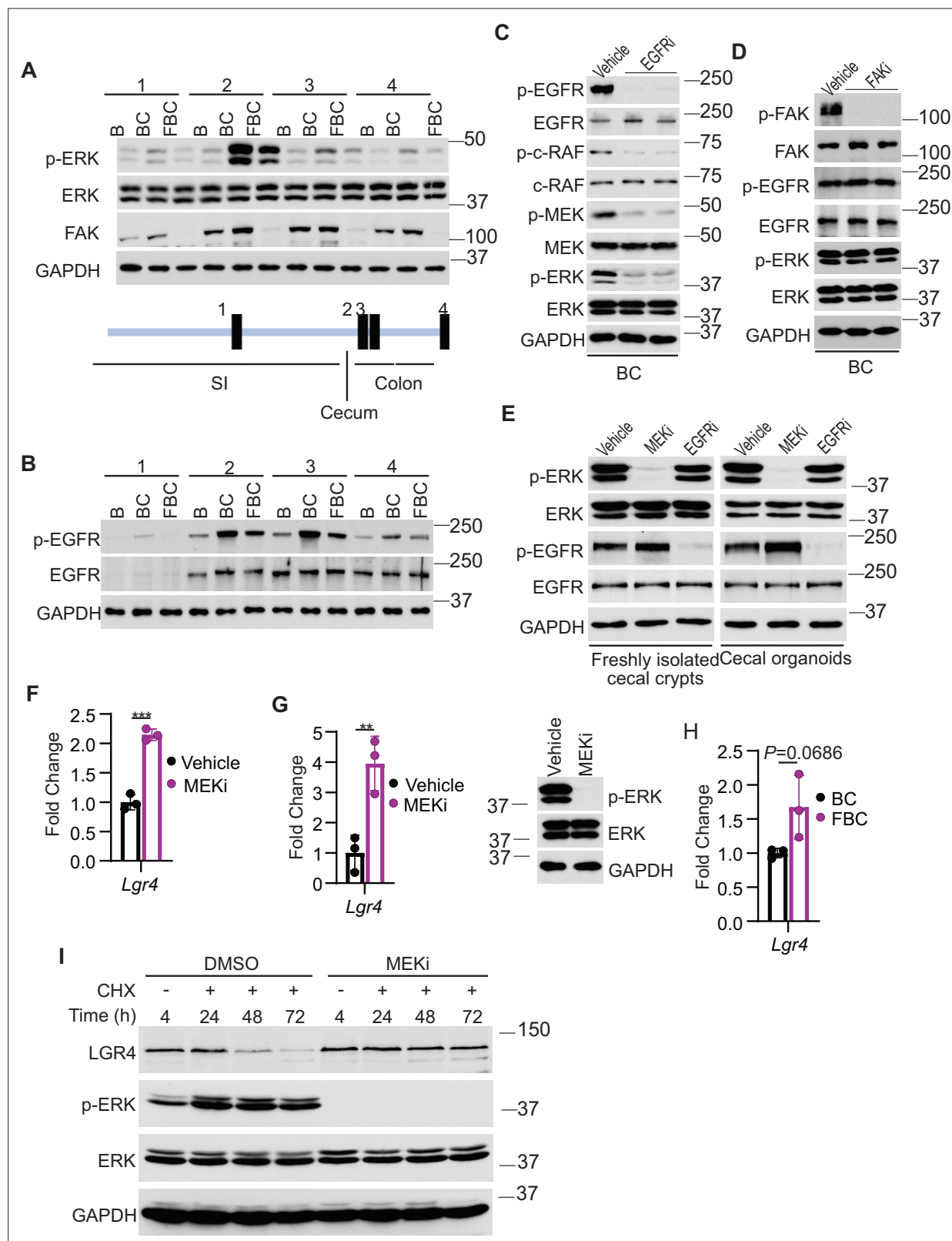


Figure 5. Fak loss inhibits ERK phosphorylation and upregulates Lgr4. (A and B) Immunoblotting analysis of intestinal mucosa lysates from indicated bowel subsites in indicated 6-week-old mice. (C) Immunoblotting analysis of cecum lysates from 6-week-old BC mice treated with vehicle or EGFR inhibitor erlotinib for 4 hr. Each lane represented a single mouse. (D) Immunoblotting analysis of cecum lysates from 6-week-old BC mice treated with vehicle or FAK inhibitor PF-562271 for 4 hr. Each lane represented a single mouse. (E) Immunoblotting analysis of lysates from freshly isolated cecal crypts and cecal organoids treated with vehicle, MEKi, or EGFRi. (F) Quantification of Lgr4 expression in cecal crypts. (G) Quantification of Lgr4 expression in cecal organoids. (H) Quantification of Lgr4 expression in cecal crypts. (I) Immunoblotting analysis of Lgr4 expression in cecal crypts treated with DMSO or MEKi, with or without CHX. Figure 5 continued on next page

Figure 5 continued

crypts and cecal organoids treated with DMSO, MEK inhibitor PD0325901, or erlotinib, respectively as described in Methods. **(F)** qRT-PCR of *Lgr4* using lysates from HT-29 cells treated with the vehicle and MEKi for 4 hr. Data presented as mean \pm SD (** $p < 0.001$; Student's *t*-test, two-tailed). **(G)** qRT-PCR of *Lgr4* using cecum lysates from BC mice treated with vehicle or MEKi for 6 hr. Data presented as mean \pm SD (** $p < 0.01$; Student's *t*-test, two-tailed). Abrogation of ERK phosphorylation at T202/Y204 in the cecum was confirmed by western blot. **(H)** qRT-PCR of *Lgr4* in cecum from BC and FBC mice ($n = 3$ per group). Data presented as mean \pm SD (p value calculated using two-tailed Student's *t*-test). **(I)** Immunoblotting analysis of the lysates from HT-29 cells treated with cycloheximide (100 $\mu\text{g/ml}$) and/or MEK inhibitor PD0325901 (10 μM) as indicated.

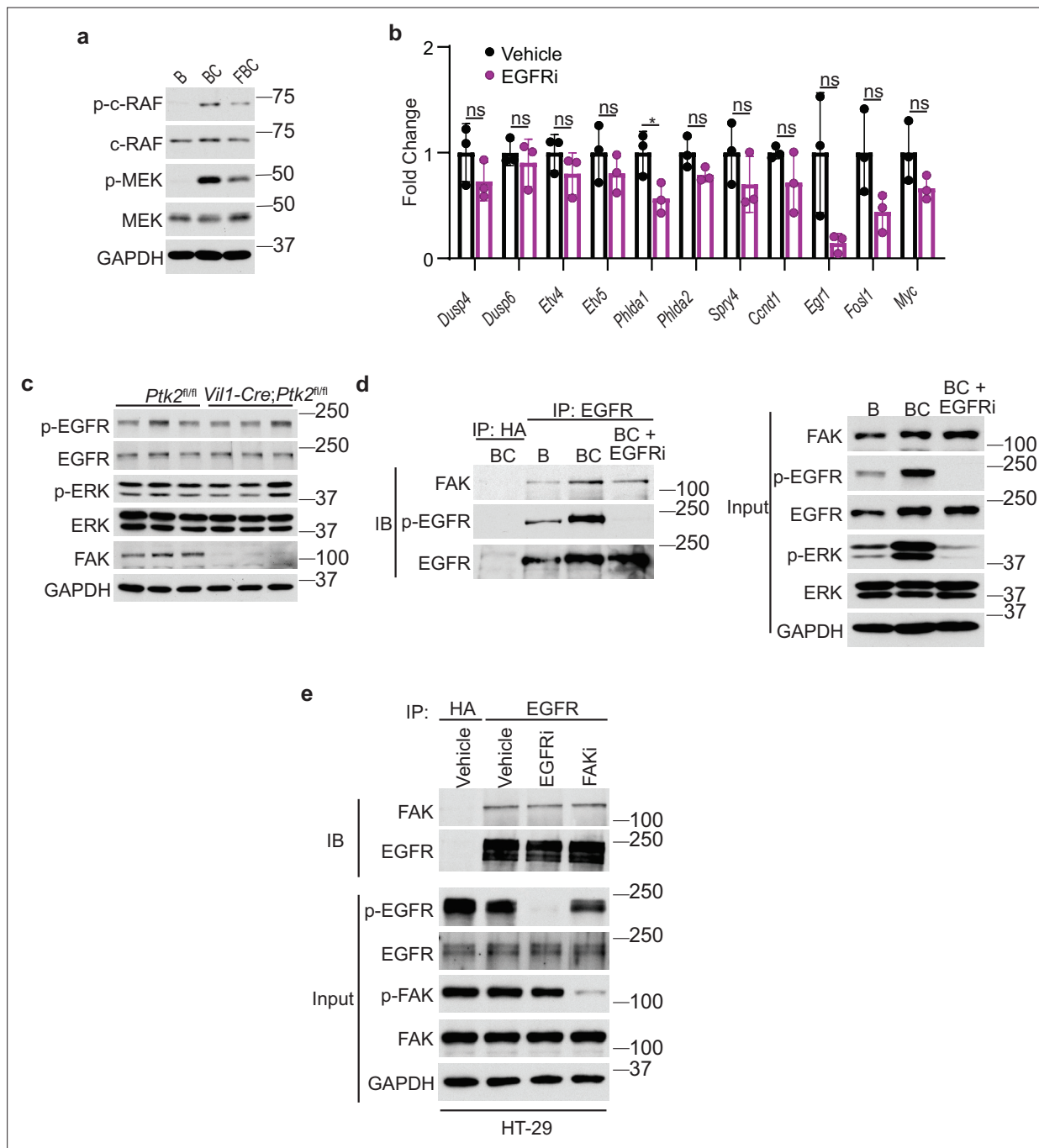


Figure 5—figure supplement 1. *Fak* loss downregulates *BRAF^{V600E}*-induced ERK phosphorylation. **(A)** Immunoblotting analysis of cecal lysates from indicated 6-week-old mice. **(B)** qRT-PCR of selected ERK transcriptional output markers in cecum from vehicle- and erlotinib-treated BC mice (n=3 per group). Data presented as mean \pm SD (ns, not significant; *p<0.05; Student's t-test, two-tailed). **(C)** The cecal mucosa lysates from 6-week-old *Ptk2^{fl/fl}* and *Vil1-Cre;Ptk2^{fl/fl}* mice were used for immunoblotting. Each lane represented a single mouse. **(D)** The cecal mucosa lysates from 6-week-old vehicle-treated B and BC mice and EGFR inhibitor erlotinib-treated BC mice were used for immunoprecipitation and immunoblotting with the indicated antibodies. **(E)** The lysates from HT-29 cells treated with vehicle, EGFR inhibitor erlotinib, or FAK initiator PF-562271 were used for immunoprecipitation and immunoblotting with the indicated antibodies.

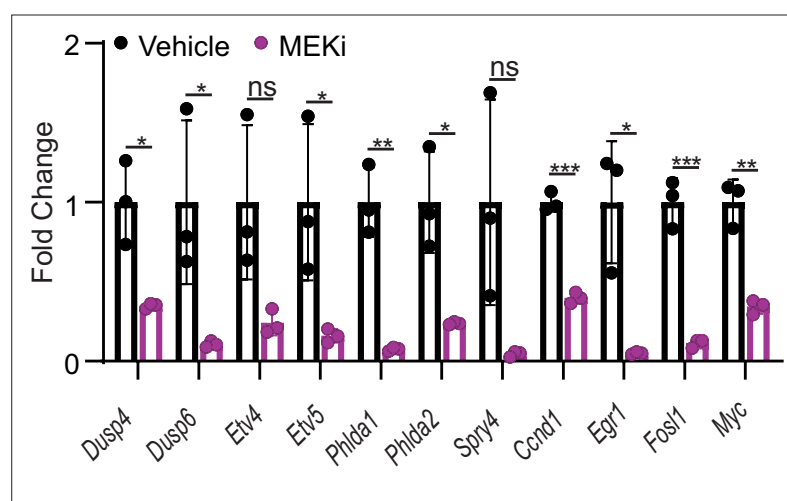


Figure 5—figure supplement 2. qRT-PCR of selected ERK transcriptional output markers in cecum from vehicle- and MEKi-treated BC mice (n=3 per group). Data presented as mean \pm SD (ns, not significant; *p<0.05; **p<0.01; ***p<0.001, Student's t-test, two-tailed).

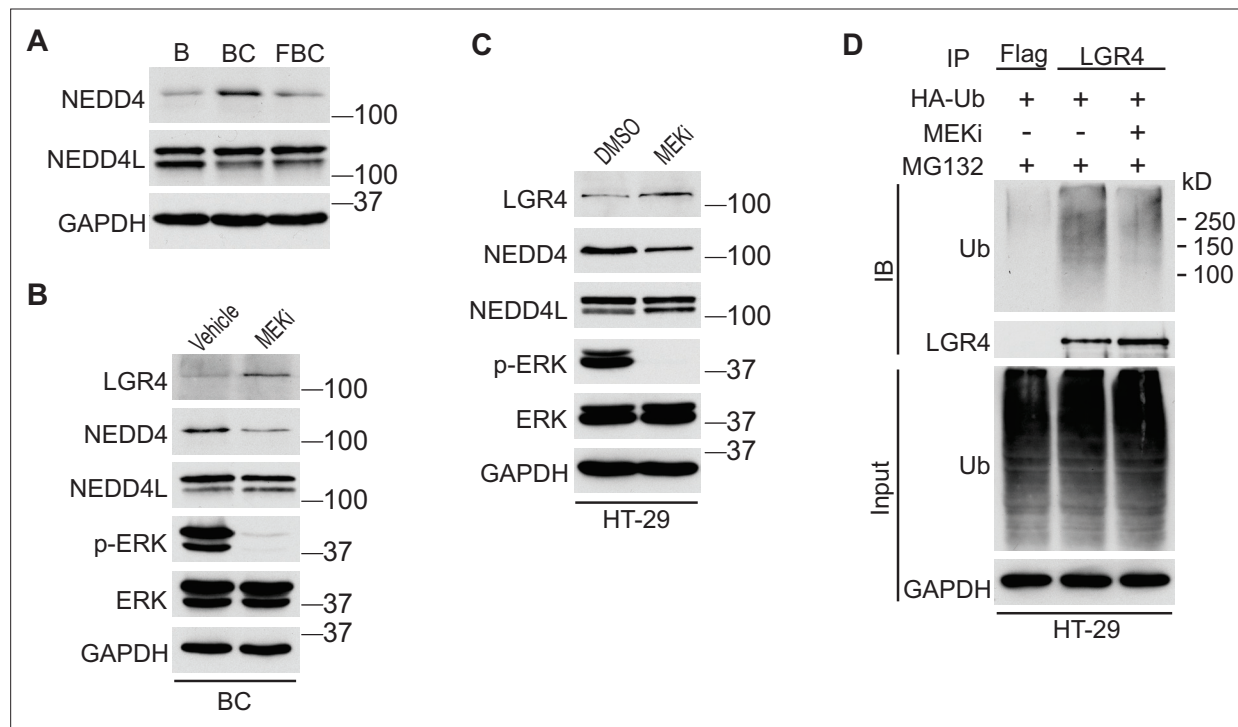


Figure 6. Inhibition of ERK phosphorylation stabilizes LGR4 through downregulating NEDD4. **(A)** Immunoblotting analysis of cecum lysates from indicated 6-week-old mice. **(B)** Immunoblotting analysis of cecum lysates from 6-week-old BC mice treated with vehicle or MEK inhibitor PD0325901. MEK inhibitor was given to the mice at a dose of 25 mg/kg three times at 12 hr intervals. Twenty-eight hours after the first treatment, the cecum mucosa was collected for immunoblotting. **(C)** Immunoblotting analysis of lysates from HT-29 cells treated with DMSO or 10 μ M MEK inhibitor for 24 hr. **(D)** HT-29 cells were transfected with HA-Ubiquitin. One day later, the cells were treated with DMSO or 10 μ M MEK inhibitor for 24 hr. Then all the cells were incubated with 10 μ M MG132 for additional 4 hr. The cell lysates were collected for immunoprecipitation and immunoblotting with the indicated antibodies.

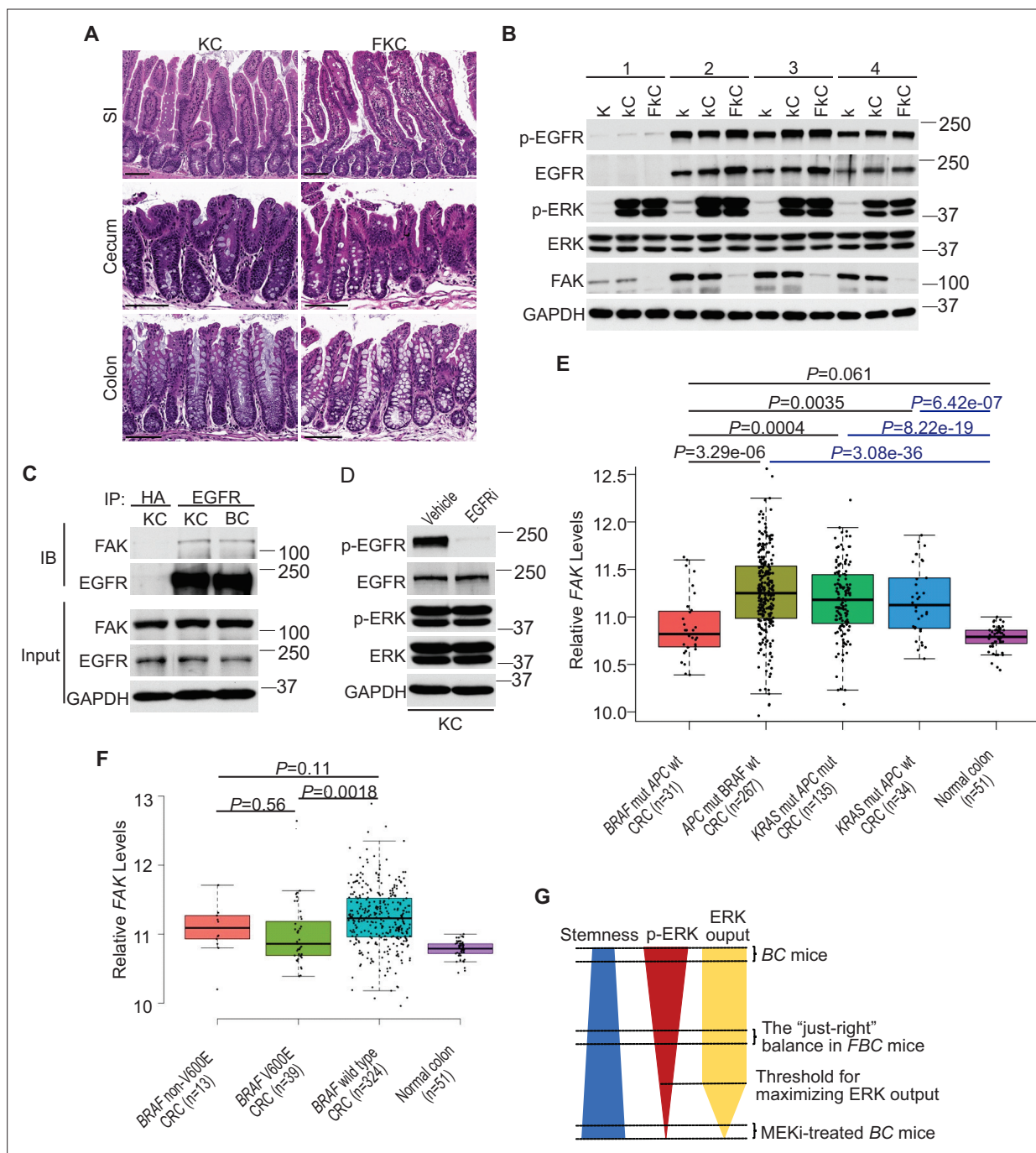


Figure 7. ERK activation is FAK/EGFR-independent in KC mice. **(A)** Representative hematoxylin and eosin (H&E) staining of the small intestine, cecum, and colon from indicated 9-month-old mice. **(B)** Immunoblotting analysis of intestinal mucosa lysates from indicated bowel subsites in indicated 6-week-old mice. **(C)** The cecal mucosa lysates from 6-week-old KC and BC mice were used for immunoprecipitation and immunoblotting with the indicated antibodies. **(D)** Immunoblotting analysis of cecal lysates from 6-week-old KC mice treated with vehicle or EGFR inhibitor erlotinib for 4 hr. **(E and F)** Comparison of FAK expression levels between CRCs with indicated mutations by analysis of TCGA RNA-sequencing dataset. Data were analyzed for statistical significance using a Student t-test. **(G)** Diagram of the 'just-right' MAPK signaling model in the serrated pathway.